Intraseasonal Oscillations in Sea Level along the West Coast of the Americas

M. C. SPILLANE, D. B. ENFIELD AND J. S. ALLEN

College of Oceanography, Oregon State University, Corvallis, OR 97331

(Manuscript received 22 April 1986, in final form 4 September 1986)

ABSTRACT

Hourly observations of coastal sea level at stations from Peru to British Columbia are analyzed for low-frequency content. A space–time contour plot of sea level, from four years of data during the 1971–75 period, shows the meridional structure of the seasonal cycle and interannual variability associated with the 1972–73 El Niño. Oscillations with intraseasonal periods of 36–73 days are also evident, coherent over alongshore distances of several thousand kilometers. Further investigation using spectral methods and empirical orthogonal function analysis in the frequency domain reveals, in particular, that intraseasonal sea level variability has a peak in spectral density along the coasts of South America, Central America and Mexico, with high coherence from near the equator (Tumaco, 2°N) north to central California (34°N) and south to at least Callao (12°S). Phase propagation north of the equator is poleward at 150–200 kilometers/day. Atmospheric pressure, alongshore wind stress and wind stress curl, derived from Fleet Numerical Oceanography Center data for the Northern Hemisphere, are used to assess the importance of local atmospheric forcing. The low coherence between sea level and these fields in the intraseasonal frequency band suggests that the observed oscillation may be a coastally propagating response to remote processes in the equatorial Pacific waveguide.

1. Introduction

Several authors have investigated large-scale coherence of sea level along the west coast of the Americas (Enfield and Allen, 1980; Chelton and Davis, 1982). For the most part these studies have employed long time series of monthly anomalies where the long-term seasonal cycle is removed. Such datasets yield information on time scales from several months to several years. Enfield and Allen (1980) employed 25 years of monthly data at stations from Chile (33°S) to Alaska (60°N). Their results indicate that interannual variability (2–5 year scales) propagates poleward from equatorial regions with phase speeds of 60–100 km day^{-1} and is coherent over alongshore scales up to 10 000 km. These prominent interannual disturbances of elevation, associated with known occurrences of the El Niño phenomenon in the tropical Pacific, are also coherent with the Southern Oscillation Index (Quinn, 1974). Idealized models (Moore and Philander, 1977; Cane and Sarachik, 1977) show that when equatorial Kelvin waves, thought to occur over a wide range of frequencies, are incident on an eastern boundary, they may be partially transmitted poleward as coastal-trapped Kelvin waves, thus providing a theoretical basis for these observations. The equatorial Kelvin waves, in turn, may originate from zonal wind changes in mid-Pacific (Wyrtki, 1975; McCreary, 1976), and the question arises as to whether similar chains of events may occur in other frequency bands.

From sea level, current and temperature records off Peru, Smith (1978) observed poleward, nondispersive propagation of perturbations with time scales of 4 to 20 days that were incoherent with local atmospheric forcing. These baroclinic coastal-trapped waves resemble internal Kelvin waves at low latitudes (Allen and Romea, 1980). Comparison of the observations with theory (Brink, 1982) confirms that most of the energy in the 5–10 day period band is due to free waves originating equatorward of 5°S. Other studies have documented the presence of free and forced propagating sea level fluctuations, with similar time scales, along the Pacific coasts of Mexico (Enfield and Allen, 1983) and the United States (Halliwell and Allen, 1984). To extend these studies of large-scale sea level variability to periods in the 20-day to one-year range, we have obtained and processed sea level records at coastal stations from Peru to British Columbia for the period 1971 to 1975.

In this paper we focus on the intraseasonal band of weeks to months. Typically this band has been neglected because it is not resolved either by monthly data or by the hourly time series of limited duration typical of most oceanographic experiments. The intraseasonal 30–70 day oscillation in the tropical atmosphere was long neglected (for similar reasons) by meteorologists until it was serendipitously discovered by Madden and Julian (1971, 1972), who had pieced together multiyear time series of synoptic weather data. Since then the atmospheric oscillation has been widely reported (Krishnamurti and Subrahmanyam, 1982; Weickmann, 1983; Mertz and Mysak, 1984). Luther (1980) found indications of an oceanic response to intraseasonal atmospheric forcing in sea level records

from islands in the equatorial Pacific. Similar findings are reported in the Gulf of Guinea (Picaut and Verstraete, 1976), and in the Indian Ocean off Kenya (Mysak and Mertz, 1984). Breaker and Lewis (1987) observed an oscillation near 46 days in sea surface temperature off central California. This midlatitude signal is coherent with local wind stress, though not with coastal sea level, and the authors speculate that atmospheric teleconnections to processes in the tropical Pacific may be involved.

In our study we document, for the first time, a very large scale latitudinal coherence of intraseasonal sea level variability at time scales near 36–73 days along the Pacific coast of the Americas, and show that ocean wave propagation is the most likely mechanism. Available atmospheric data for the coastal region are not found to exhibit organized structures of comparable spatial extent at similar time scales.

A full description of the sea level and atmospheric data is given in section 2. The space–time structure of sea level is discussed in section 3, together with the distribution of energy in the frequency domain. In sections 4 and 5 we use cross-spectral analysis and frequency-domain empirical orthogonal function (EOF) analysis to describe the intraseasonal band. The available meteorological data are analyzed in section 6 to look for possible sources of forcing, and the results of the study are summarized in section 7.

2. Data

Tide gauge records for the years 1971 to 1975 were obtained from several sources as detailed in Table 1. A four-year period (beginning and ending in mid-April), with only minor gaps, is common to all tide stations. Three-letter abbreviations, defined in Table 1, are used to identify the stations in the figures. The disposition of stations is shown on a Mercator projection in Fig. 1. A smoothed representation of the coastline is used to define an alongshore distance scale with its origin at the equator. Notice that the station distribution is skewed in favor of the Northern Hemisphere, and that over 10 000 km of coastline are represented.

The hourly data are first screened for errors and datum shifts. Neighboring stations, not otherwise used in the analysis, are employed to fill data gaps when available. In the absence of such additional data, short gaps (of less than 13 days) are bridged by autoregression (Box and Jenkins, 1970). This technique uses an algorithm by Andersen (1974) to compute prediction error filters, based on the statistical properties of the valid data preceeding and following each gap. These filters provide the autoregressive parameters necessary for extrapolation from both ends into the region of missing data. The two predictions for each missing value, weighted in inverse proportion to the extrapolation distance, are added thereby bridging the gap without

TABLE 1. List of sea level stations for which hourly tide gauge records are available. With the exception of those indicated by an asterisk (not used in the main analysis), the records span a four-year period during 1971–75, beginning and ending in mid-April. Three-letter codes used to abbreviate station names in figures are defined, together with an alongshore distance scale (kilometers), with origin at the equator, based on a smoothed representation of the coastline. Data sources are: National Ocean Survey (NOS); Centro de Investigación Científica y de Educacion Superiór de Ensenada (CICESE); Universidad Nacional de Costa Rica (UNCR); Instituto Oceanografico de la Armada (INOCAR); Direccion de Hidrografia y Navegación de la Marina (DHNM); Instituto Geográfico Agustín Codazzi (IGAC); Institute of Ocean Science, Canada (IOS); and Panama Canal Co. (PCC).

Station	Code	Latitude	Longitude	Distance (km)	Data source
Prince Rupert	PRR	54°19′N	130°19′W	9040	IOS
Neah Bay	NBA	48°22′N	124°37′W	8255	NOS
South Beach	SBC	44°38′N	124°03′W	7840	NOS
Crescent City	CCY	41°45′N	124°12′W	7515	NOS
San Francisco	SFO	37°48′N	122°28′W	7030	NOS
Monterey	MRY	36°36′N	121°54′W	6880	NOS
Los Angeles	LOS	33°43′N	118°16′W	6375	NOS
Ensenada	ENS	31°51′N	116°38′W	6075	CICESE
La Paz	LPZ*	24°00′N	110°15′W	—	CICESE
Guaymas	GUY*	27°49′N	110°58′W	—	CICESE
Topolobampo	TOP*	25°45′N	109°00′W	—	CICESE
Mazatlan	MAZ	23°12′N	106°25′W	4800	CICESE
Manzanillo	MNZ	19°03′N	104°20′W	4275	CICESE
Acapulco	ACA	16°51′N	99°55′W	3775	CICESE
Salina Cruz	SCZ	16°10′N	95°12′W	3275	CICESE
San Jose	SJO	13°55′N	90°50′W	2725	UNCR
Quepos	QPO	9°24′N	84°10′W	1875	UNCR
Balboa, C.Z.	CZN	8°58′N	79°34′W	1200	PCC
Tumaco	TCO	1°50′N	78°44′W	300	IGAC
La Libertad	LLB	2°12′S	80°55′W	−250	INOCAR
Talara	TAL	4°37′S	81°17′W	−500	DHNM
Callao	CAL	12°03′S	77°09′W	−1500	DHNM

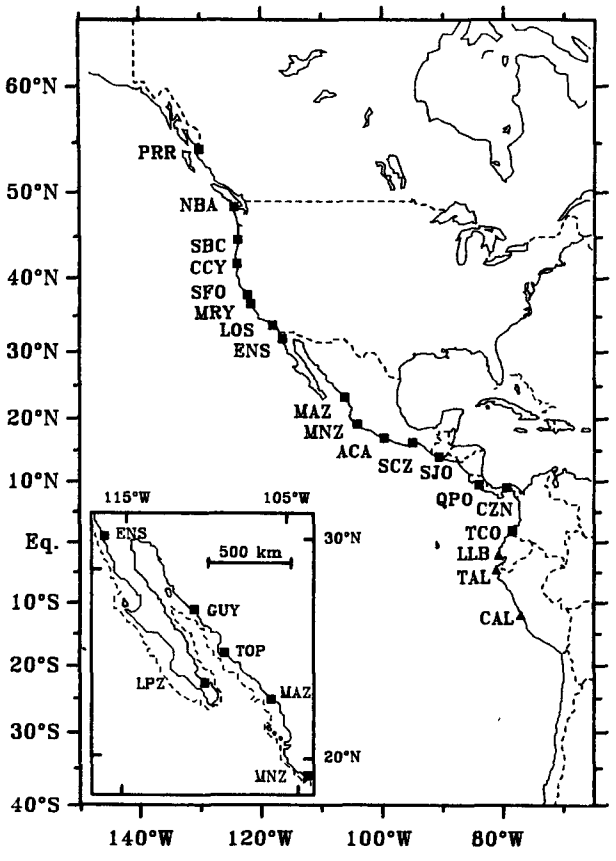

FIG. 1. Sea-level station locations for the 1971–75 period. Triangles show stations for which sea level data alone are available, while squares indicate those for which FNOC atmospheric pressure data exist, allowing the computation of adjusted sea level. Inset with an expanded scale is the region near the mouth of the Gulf of California. The 1000 m isobath is shown as a dashed line. Data from the stations at La Paz, Guaymas and Topolobampo are not employed in the main analysis but are discussed in section 5.

discontinuities. Such bridging allows us to use records of uniform length in our analysis, but affects only a small percentage of the data at any station.

The records at Talara and La Libertad each contain two larger gaps that cannot be reliably bridged in this manner. The gaps (24 and 40 days at Talara; 33 and 22 days at La Libertad) are not simultaneous and each station is patched using data from the other, adjusting the local trend to ensure continuity. These insertions amount to 6% and 4%, respectively, of the records. Tests on the longest gap-free section (864 days) indicate that insertions of less than 10% of the record length do not significantly alter estimates of coherence, phase or spectral density.

The resulting records are low-pass filtered to remove the semidiurnal and diurnal tides. The Cosine–Lanczos filter used has a half-power point at 46 h. The characteristics of this filter have been compared to other commonly used low-pass filters by Beardsley et al. (1985). Decimation to daily values produces a 1458 point series (three days less than the full four years) at each station, with common start time at 0000 UTC April 16.

Direct measurements of atmospheric forcing parameters are not readily available over the entire geographic region. Instead, as in earlier studies (Enfield and Allen, 1980; Halliwell and Allen, 1984) we utilize the gridded atmospheric pressure data produced by the Fleet Numerical Oceanography Center (FNOC), and the wind stress and wind-stress curl fields derived from it. Six-hourly atmospheric pressure data from FNOC are available only for the Northern Hemisphere stations, and the gridded pressures are interpolated to sea-level station locations. Where available, the atmospheric pressure has been added (with a scale factor of 1 cm/mb) to sea level height to form the adjusted sea level. Sea level adjusted in this manner is a measure of the total subsurface pressure, and as such relates to the dynamics of the upper ocean.

Surface wind speed components are calculated from the pressure field in the manner described by Bakun (1973). From these the wind stress is obtained using the bulk aerodynamic formula, with the drag coefficient of Large and Pond (1981). The calculated stress represents a large-scale average over a grid element spanning three degrees in both latitude and longitude. A more complete description of the preparation of these wind data is given by Halliwell and Allen (1984). The orientation of the smoothed coastline at each grid point defines the alongshore (positive poleward) component of wind stress. The angles used are listed in Table 2. Also available from the gridded data is the wind stress curl. Pressure, wind stress and wind stress curl records are filtered and decimated in conformity with the sea level series.

The reliability of geostrophic computations of the wind field from pressure data decreases near the equator. Some two years of measured wind stress data are available at Salina Cruz (16°N). The measured and calculated series are highly correlated, at above the 99.9% significance level, with the highest correlation (0.78) occurring at zero lag. The standard deviation of the calculated stress exceeds that of the measured stress by a factor of 2.5, implying an overestimation of wind speed by some 60%. When scaled down in proportion to the variance difference, the autospectrum for calculated wind stress is in close agreement with that of measured stress over the period range 5–182 days. The series are coherent above the 90% significance level (0.32) over this entire period range, while for the longer periods (greater than 30 days) the coherence exceeds the 99% significance level (0.54). Wind measurements are available also at Acapulco (17°N). Though farther from the equator, the comparison with calculated winds is very poor. It would appear that local orographic influences may be responsible, and further study of the relationship between calculated and measured winds at low latitudes would be desirable. We utilize calcu-

TABLE 2. Statistics of sea level, FNOC pressure and alongshore wind stress for the four-year period beginning 16 April 1971. Tabulated are the standard deviations for measured sea level, adjusted sea level and atmospheric pressure; the mean and standard deviation of wind stress; and the cross-correlation coefficients for adjusted sea level and pressure (r_{sp}), adjusted sea level and alongshore wind stress (r_{sw}), and pressure and wind stress (r_{pw}). Asterisks indicate correlations below the 90% significance level while those above the 99% level are shown in boldface. The degrees of freedom used to establish significance levels are based on integral time scales (Davis, 1976). The coastline orientations used to decompose wind vectors are given as the counterclockwise angle (degrees) from east to the alongshore direction.

Station code	Coastline orientation (deg)	Measured sea level (cm)	Adjusted sea level (cm)	Atmospheric pressure (mb)	Alongshore windstress (N m^{-2})		r_{sp}	r_{sw}	r_{pw}
PRR	120	14.8	8.1	9.6	0.82	2.08	**−0.87**	**0.44**	**−0.27**
NBA	120	17.3	12.8	7.6	0.34	1.13	**−0.73**	**0.50**	**−0.34**
SBC	85	16.0	12.5	6.5	0.15	1.13	**−0.68**	**0.63**	**−0.36**
CCY	103	13.2	10.5	5.6	−0.11	1.36	**−0.65**	**0.56**	**−0.26**
SFO	102	9.3	8.3	4.8	−0.38	0.87	**−0.45**	**0.46**	*
MRY	128	7.6	6.6	4.6	−0.44	0.76	**−0.52**	**0.39**	*
LOS	150	7.4	6.5	4.0	−0.54	0.54	**−0.46**	*	0.28
ENS	110	7.7	6.7	3.7	−0.32	0.28	−0.47	*	*
MAZ	126	13.4	12.7	2.3	−0.12	0.53	−0.36	0.22	**0.26**
MNZ	135	11.4	11.0	1.9	−0.03	0.50	−0.26	0.23	**0.18**
ACA	160	11.7	11.2	2.0	0.20	0.91	−0.24	*	**0.43**
SCZ	167	13.0	12.1	2.2	0.40	1.35	**−0.44**	**−0.35**	**0.59**
SJO	156	10.4	10.1	1.6	0.47	1.06	−0.17	*	**0.50**
QPO	142	9.7	9.3	1.3	0.35	0.80	−0.27	*	*
CZN	180	12.4	12.1	1.3	0.43	0.79	−0.23	**−0.56**	0.16
TCO	—	10.0	9.7	1.3	—	—	*	—	—
LLB	—	8.4	—	—	—	—	—	—	—
TAL	—	8.3	—	—	—	—	—	—	—
CAL	—	8.5	—	—	—	—	—	—	—

lated winds as far south as Canal Zone (9°N) since it is the only data available, but one must bear in mind the possibility of inaccuracies at low latitudes.

The basic statistics of sea level, atmospheric pressure and alongshore wind stress variability are summarized in Table 2 for the four-year period of the present study. Also indicated are the correlation coefficients between sea level and the meteorological variables. The degrees of freedom appropriate to each correlation are computed from the integral time scale (Davis, 1976). Only those correlations significant above the 90% level are tabulated, with values exceeding the 95% significance level indicated in boldface text. As reported by Enfield and Allen (1980) and Chelton and Davis (1982) for monthly mean data, daily atmospheric pressure becomes less energetic, and less correlated with sea level, with decreasing northern latitude. Smith (1978) noted that coastal atmospheric pressure fluctuations along the Peru coast are weak also, and poorly correlated with sea level variations. These facts support the combined use of adjusted (Northern Hemisphere) and unadjusted (Southern Hemisphere) sea level series in our analysis.

3. Spatial structure of sea level variability

Deviations from the mean of adjusted sea level are displayed in Fig. 2 as a space–time contour plot. For clarity, the time series were further smoothed with a low-pass filter (20-day cutoff, 30-day half-amplitude) for this presentation only. A strong seasonal cycle is clearly evident. At lower latitudes heating effects dominate, causing sea level to be high in summer and low in winter. North of San Francisco steric effects are secondary to the influence of the wind and the highest sea level occurs in winter, when poleward winds are strongest. The 1972–73 El Niño appears as an amplification of the regular cycle, and the aborted 1975 El Niño is also visible at the three southernmost stations. Within seasons, features with periods of about two months are evident that are correlated over scales of several thousand kilometers. Visual estimates indicate poleward propagation speeds of 150–200 km day^{-1}. These intraseasonal signals are further investigated in the following sections. The lower panel of Fig. 2 is discussed in section 5.

Spectral analysis is used to investigate the frequency content of the sea level records. The autospectral density of adjusted sea level is shown in Fig. 3, with estimates from seven adjacent Fourier frequencies combined in a moving band average. The 95% confidence range (appropriate to 14 degrees of freedom) is indicated in the panel on the right. Although the spectrum is red, it has a strong peak at frequencies centered near 0.02 cycles per day (cpd), i.e., periods of about 50 days. As noted by Madden and Julian (1971) the significance of a spectral peak for which there is no a priori dynamical expectation should be judged more stringently than by the usual chi-squared sampling limits. For an a posteriori test of the intraseasonal peak we examine a wider band of 21 frequencies, with period range 36–73 days. When the cosine tapering, applied during the formation

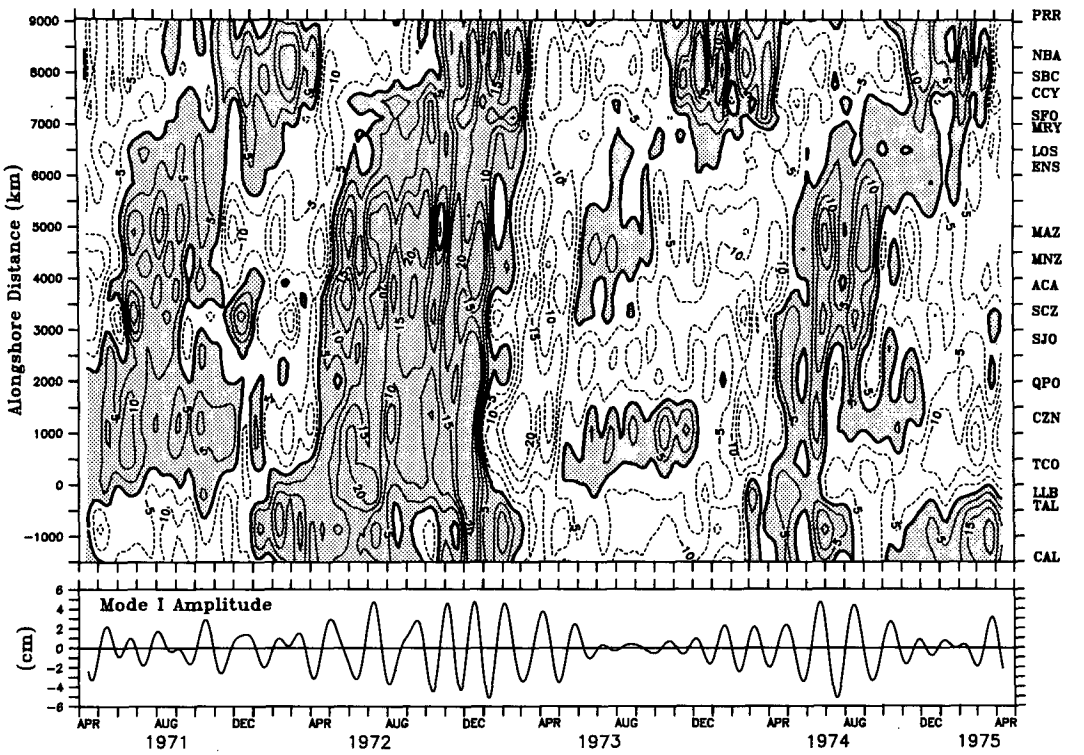

FIG. 2. Space-time contour plot of sea level deviations from the local 4-year mean, 1971–75 (above). Data have been smoothed with a low-pass filter (20 day cutoff, 30-day half-amplitude). Positive deviations are shaded, and contour levels expressed in centimeters. The lower panel shows the time history of the frequency domain EOF mode for intraseasonal band poleward propagation, as discussed in section 5.

of spectral estimates, is taken into account there are effectively 37 degrees of freedom associated with this band. A test statistic of $\chi^2(0.1\%)/37 = 1.87$ is chosen as a measure of significance. For peak values in the sample spectrum exceeding the background by a factor of 1.87 the a posteriori confidence limit (i.e., the probability of a chance occurrence of any such peak) is approximately 3.5%. With the exception of Tumaco, the station nearest the equator, all stations from Callao to Manzanillo have intraseasonal peaks exceeding this criterion. The simultaneous occurrence of the peak at several stations, together with other nonstatistical features conforming with theoretical expectation for a coastal trapped wave (see subsequent sections), further increases our confidence in its reality.

The peak falls below the confidence limit at the entrance to the Gulf of California. Comparison of the spectra at Mazatlan (23°N) and Ensenada (32°N) suggests that, as seen for the hurricane-induced, higher frequency signals investigated by Enfield and Allen (1983) and Christensen et al. (1983), energy at periods up to 150 days is strongly attenuated by the Gulf. Subsequent cross-spectral analysis will show, however, that a detectable portion of the 36–73 day signal does extend to Ensenada and beyond. Farther north, the higher frequency energy picks up due to synoptic-scale atmospheric variability. Additional comments on the distribution of spectral energy will be made later.

4. Cross-spectral analysis

The spectral estimates for all stations, when combined, form the cross-spectral matrix. From this we may extract the coherence and phase spectra relative to a single station. Using Quepos, Costa Rica, as the base station, the leftmost panel of Fig. 4 shows that, for periods near 50 days, a lobe of high coherence extends from Peru in the south past the Gulf of California to San Francisco in the north. The ridge of high coherence coincides in frequency with the peak of higher energy referred to in Fig. 3, but the region of clear expression extends farther to the north.

Selecting a band within this lobe (47–58 days, 14 degrees of freedom), the phase distribution plotted in the third panel of Fig. 4 is consistent with poleward propagation from the tropics into both hemispheres. Error bars indicate the 95% confidence interval for phase at stations where the coherence (center panel) is significant. The phase speed, computed from a least-squares fit to the section indicated, is 143 km day^{-1}, with a 95% confidence range of ±17 km day^{-1}. Poleward propagation extends to Crescent City in northern

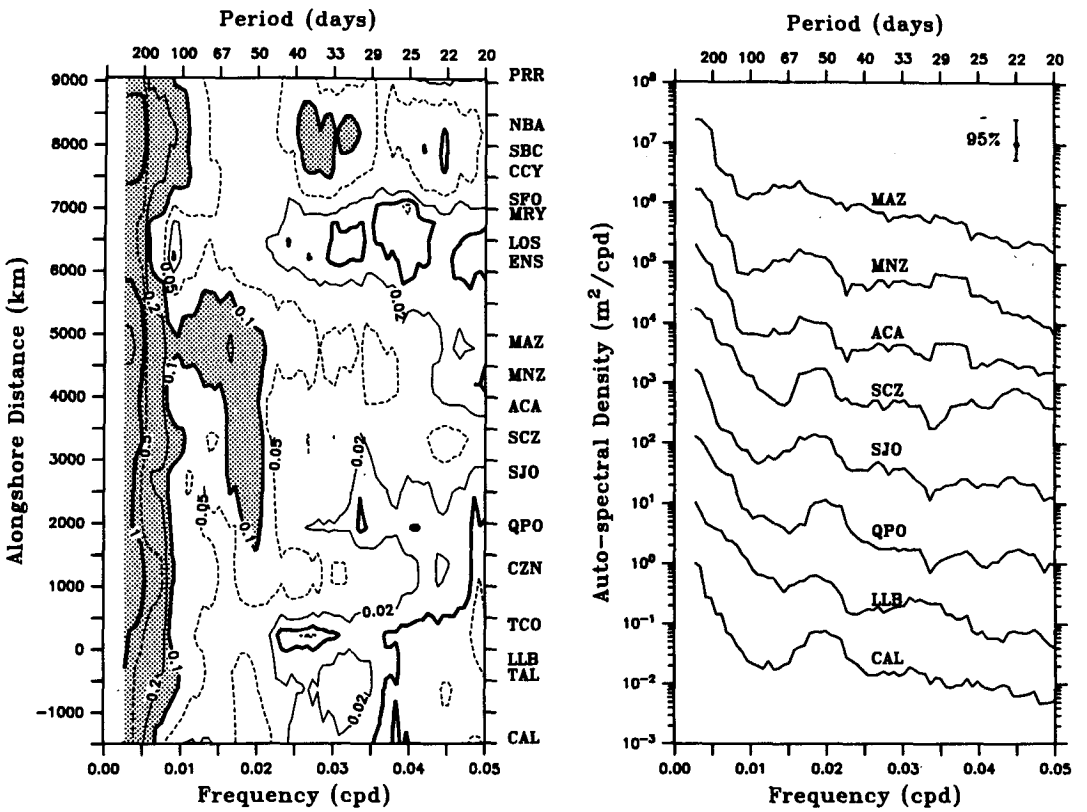

FIG. 3. Spatial structure of the autospectral density of sea level. Estimates have 14 degrees of freedom in a moving average. Contour levels (left), in approximately logarithmic steps (1, 2, 5, 10), are expressed in units of m^2 cpd^{-1} with values above 0.1 shaded. Multiplication of an autospectral estimate by 2.73 and 0.51 provide the upper and lower 95% confidence limits. Transects (right) at selected stations further illustrate the structure of the intraseasonal peak. The vertical axis is drawn for Callao, with successive stations offset by a decade for clarity.

California despite the drop in coherence at San Francisco. Schott and Düing (1976) have suggested that phase estimates for a coherent signal in a background of noise are more robust than the coherence. In autospectral averages the effects of noise are additive while some cancellation is to be expected in co- and quad-spectral averages. As a result, noise tends to reduce coherence estimates due to the autospectral terms in the denominator, while in phase estimates, where only the co- and quad-spectra appear, the influence of noise tends to average out.

Another presentation, that retains all the information in the cross-spectral matrix for a selected frequency band, is illustrated in Figs. 5 and 6. By contrast, Fig. 4 displays only a single column of the matrix. The coherence-squared matrix for the 47–58 day band is displayed in Fig. 5. As in Fig. 4, contour levels are drawn for the 90%, 95% and 99% significance levels appropriate to 14 degrees of freedom. Shading is used to highlight coherences exceeding the 95% level. Starting with a station on the diagonal, points that lie below show the coherence of that station with stations to the south. Points to the left show the coherence with stations to the north. Very high coherence can be seen for the entire region between Canal Zone and Los Angeles, and, with the exception of some pairings with Canal Zone, significant large-scale coherence also extends southward as far as Callao. There is a coherence gap over northern California and Oregon, perhaps associated with locally forced fluctuations. Breaker and Lewis (1987) have observed an intraseasonal sea surface temperature oscillation near San Francisco, coherent with the alongshore wind stress, and speculate on possible atmospheric teleconnections with the tropics. Neah Bay is coherent with a number of stations south of Monterey. Prince Rupert in British Columbia is coherent only with those stations immediately to its south. Its location, on an inlet sheltered by offshore islands, is not ideal for the study of coastal-trapped waves. Overall, Fig. 5 shows that coherence scales of 4000–6000 km are not uncommon in the 47–58 day band.

Figure 6 is a matrix plot of the phase spectrum in the 47–58 day band. Contoured is the phase lag in days of each station on the diagonal with stations below it (i.e., farther to the south). Its interpretation is aided by reference to the schematic insert. Propagation at con-

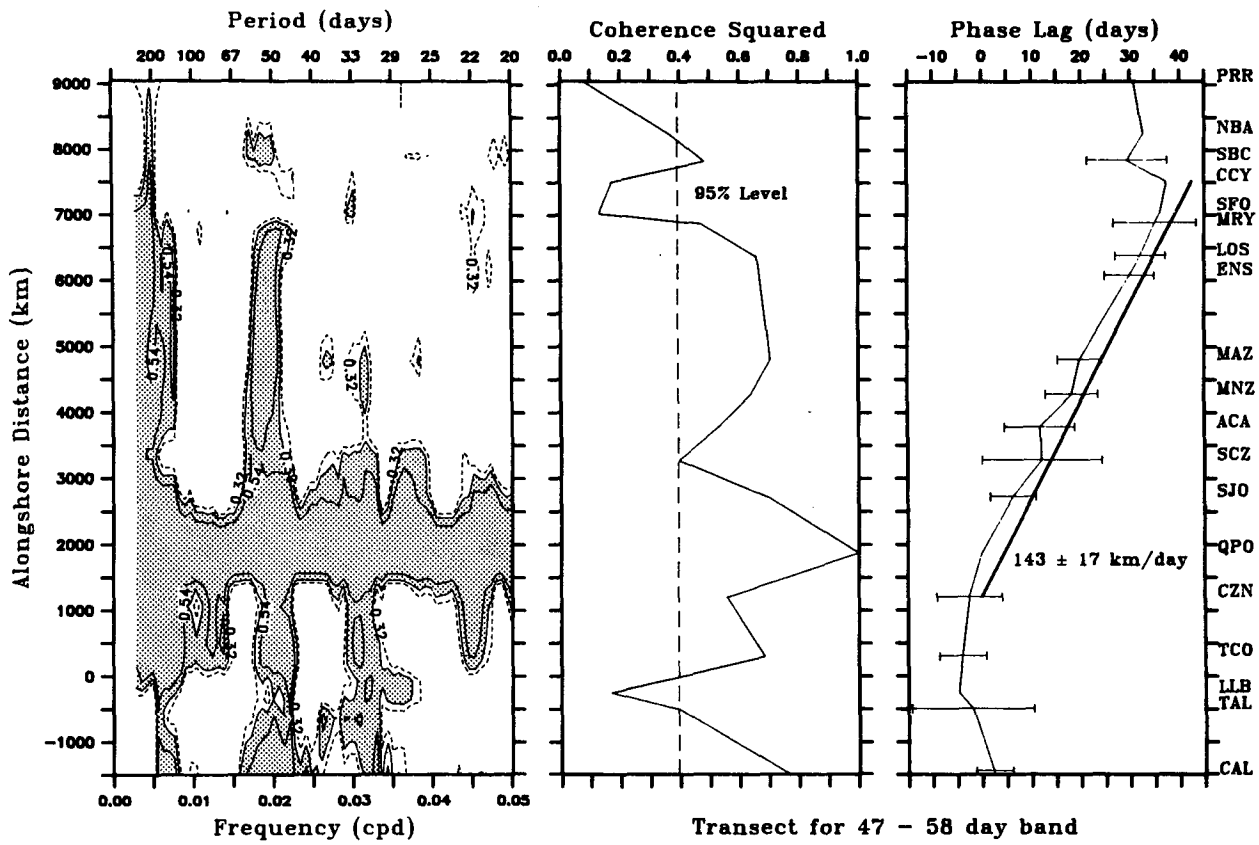

FIG. 4. Coherence squared of sea level relative to Quepos, Costa Rica (9.4°N). Contour levels (left) are drawn at 0.32, 0.39 and 0.54, corresponding, for 14 degrees of freedom, to the 90%, 95% and 99% significance levels. Shaded areas denote coherences above the 95% level. The center and right panels show a transect for the 47–58 day band. Error bars indicate the 95% confidence range for phase estimates, for stations where the coherence exceeds the 95% significance level.

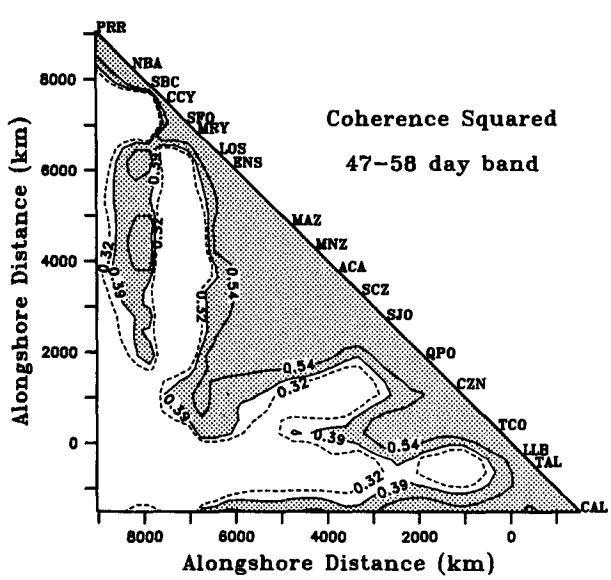

FIG. 5. Space–space contour plot of the coherence matrix for sea level in the 47–58 day band. Contour levels are as in Fig. 4, with coherences above the 95% significance level shaded.

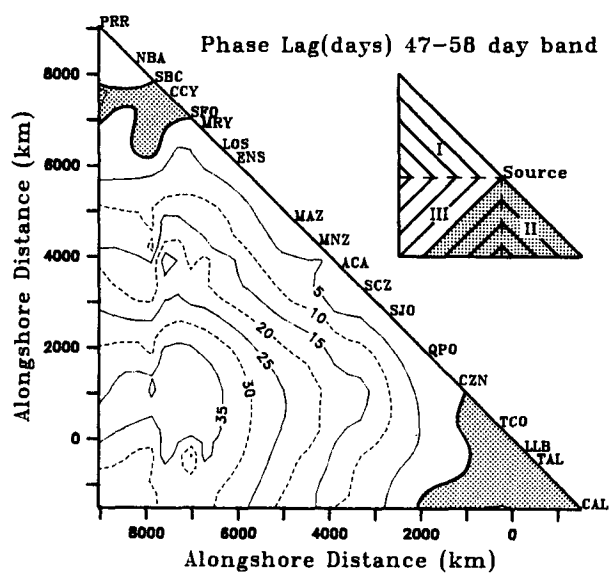

FIG. 6. Space–space contour plot of the phase-lag matrix for sea level in the 47–58 day band. See text discussion of the inset at upper right for interpretation. Shading indicates negative phase lags and contour levels are expressed in days.

stant speed in both directions from a point source would result in phase contours paralleling the diagonal in the triangular regions I and II, with positive and negative lag values, respectively. The rectangular region III contains station pairs spanning the source. Phase lag contours in this region should lie perpendicular to the diagonal, with the zero-lag contour passing through the source. The pattern of observed phase, over most of the geographic domain, is consistent with a poleward propagation from a near-equatorial source of energy in the 47–58 day band. The phase speed appears to be quite uniform until the pattern breaks down north of Los Angeles. The general features of Fig. 6 are repeated, with similar phase speed though decreased clarity, for frequency bands adjacent to the 47–58 day band. The phenomenon of strong poleward-propagating disturbances of equatorial origin appears to span the period range 36–73 days.

5. Empirical orthogonal function analysis

Frequency-domain empirical orthogonal functions are another useful representation of the results of the cross-spectral analysis. The technique (Wallace and Dickinson, 1972) isolates the principle modes of covariability for the entire set of stations within a chosen frequency band, and preserves information about the relative phase. For the 47–58 day band a single mode dominates, accounting for 72% of the total variance. The variance explained, rms amplitude and phase structures for this mode are shown in Fig. 7. More than 50% of the variance in the band is explained by the first mode at all stations between Monterey and the equator.

The phase structure of the Mode I eigenvector again indicates poleward propagation from the equatorial region. Enfield and Allen (1983) computed phase speeds for coastal sea level fluctuations between San Jose (13°N) and Mazatlan (23°N) from cross-spectral estimates in the 7–50 day period range, and compared their results with the predictions of linear theory using the model of Brink (1982). Based on measured hydrographic profiles and bottom topography the average theoretical phase speed of coastal-trapped waves in this region is 190 km day^{-1}, with negligible seasonality. The model does not include bottom friction. Theoretical

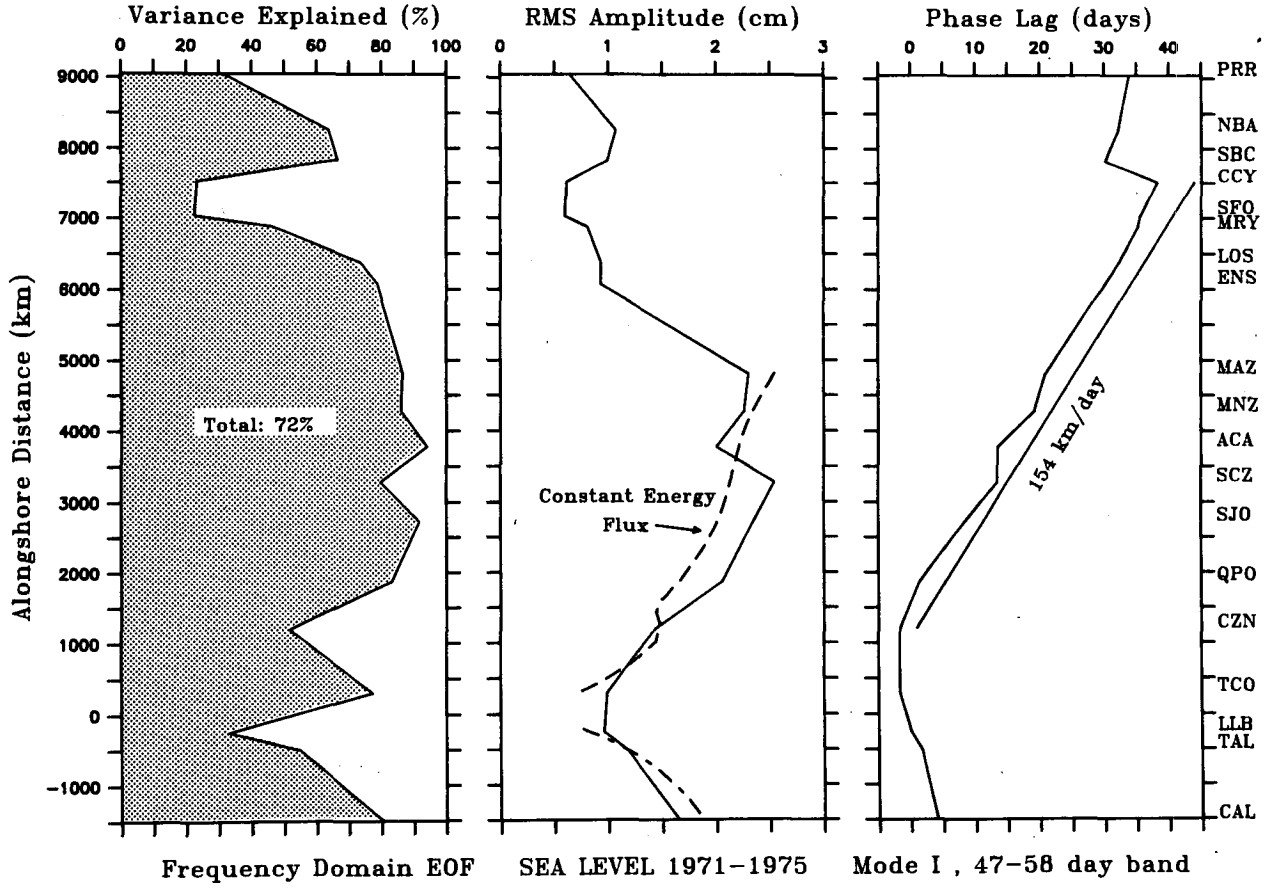

FIG. 7. Frequency domain EOF for sea level in the 47–58 day band. This poleward propagating mode accounts for 72% of the variance in the band. The dashed curve of the center panel is discussed in the text.

considerations by Allen (1984) have shown that friction causes a slight reduction in phase speed for low-frequency coastal-trapped waves. The phase speed computed from the 47–58 day band EOF mode shown in Fig. 7 is 154 km day^{-1} over the region indicated, and 167 km day^{-1} between San Jose and Ensenada, in approximate agreement with theoretical predictions. Another feature of note in Fig. 7 is the region of near-constant phase close to the equator between Canal Zone (9°N) and Talara (4.6°S). This is qualitatively consistent with theoretical predictions for low-frequency coastal-trapped waves at low latitudes (Cane and Sarachik, 1977).

The root mean square (rms) amplitude distribution for the Mode I eigenvector is in agreement with the spectral density at the appropriate frequency (0.019 cpd) in Fig. 3. A feature of note is the lower rms amplitude in the tropics. If this is the source region for poleward-propagating signals, one might expect the amplitude to be maximum there. However, in this region the latitudinal variation of the Coriolis parameter causes the coastal deformation radius to decrease rapidly with latitude. The resulting confinement of energy to a narrowing offshore zone should cause an increase in amplitude with distance from the equator (Moore and Philander, 1977). Coastal-trapped internal Kelvin wave theory, with negligible friction and uniform equivalent depth, requires that coastal sea-level amplitudes vary as the square root of the Coriolis parameter to maintain constant energy flux (e.g., Gill, 1982). The dashed curve, in the center panel of Fig. 7, indicates the predicted rms amplitude structure for the Pacific coastline as far north as Mazatlan. Talara (4.5°S) lies outside the equatorial deformation radius, and is used as a reference level. The qualitative agreement with the amplitude structure of the EOF mode is evident.

The drop in amplitude in the intraseasonal band between Mazatlan and Ensenada was referred to earlier. The signal does remain detectable, however, in both amplitude and phase as far as mid-California. This contrasts with higher frequency, hurricane-induced signals (Christensen, 1983; Enfield and Allen, 1983), which are effectively blocked by the Gulf of California. At the other extreme, interannual signals are of such low frequencies that, even at the latitude of the mouth of the Gulf of California, they are not coastally trapped (Cane and Sarachik, 1977), and as seen by Enfield and Allen (1980) and Chelton et al. (1982), the Gulf of California poses no obstacle.

In Table 3 spectral information for stations in the vicinity of the Gulf of California is listed. The common period is limited to 728 days, due to missing data at La Paz. Station locations are indicated in the inset panel of Fig. 1, where the dashed line represents the 1000-m isobath. Spectral quantities are evaluated for the 36–73 day band with 22 degrees of freedom. Autospectral densities, tabulated on the diagonal of Table 3, show that the intraseasonal signal drops by about half in amplitude between the mainland stations (Manzanillo to Guaymas) and La Paz on the eastern side of the Baja peninsula. As noted by Christensen et al. (1983), much of the energy entering the Gulf of California appears to be dissipated in its upper reaches. The pattern of phase lags between stations show a consistent pattern of counterclockwise propagation within the Gulf, whose width greatly exceeds the frequency-corrected deformation radius (30 km). However, while stations within the Gulf are highly coherent, it should be noted that the coherence to Ensenada decreases in going from Manzanillo to Guaymas, i.e., for stations farther into the Gulf, and La Paz is not coherent with Ensenada. Hence although the 36–73 day spectral densities are similar at La Paz and Ensenada, it is unlikely that coastal-trapped waves completing the circuit within the Gulf are responsible for the signal seen at Ensenada and beyond. The ratio of the separation between Manzanillo and Ensenada to their phase difference is 205 km day^{-1}, close to the phase speed of 190 km day^{-1}, computed by Enfield and Allen (1983) using the model of Brink (1982). The picture that emerges is that the intraseasonal coastal-trapped wave energy divides north of Manzanillo with the major portion entering the Gulf of California and the remainder continuing northward along the Pacific coast of the Baja peninsula. Diffraction of Kelvin waves at a gap, or across the mouth of an inland sea, has been extensively treated by several authors (e.g., Buchwald and Miles, 1974). Since the gap between the islands north of Man-

TABLE 3. Summary spectral information at stations in or adjacent to the Gulf of California (see inset to Fig. 1) for the 36–73 day band during the period 3 January 1973 to 31 December 1974. Estimates have 22 degrees of freedom. On the diagonal are autospectral densities in units of cm^2 cpd^{-1}. Upper and lower confidence limits are obtained by multiplying the tabulated values by factors of 2.04 and 0.59. In the upper right are coherence squared estimates for all station pairs, with 90%, 95% and 99% significance levels at 0.21, 0.26 and 0.37, respectively. Phase differences in days are shown in the lower left, positive values indicating that the station at the head of the column leads.

	MNZ	MAZ	TOP	GUY	LPZ	ENS
MNZ	791	0.88	0.57	0.69	0.31	0.39
MAZ	0.7	908	0.66	0.75	0.41	0.34
TOP	3.9	2.9	665	0.87	0.48	0.24
GUY	4.1	3.2	0.3	759	0.42	0.25
LPZ	10.4	10.8	8.6	8.7	221	0.08
ENS	8.8	8.5	6.2	5.7	0.2	188

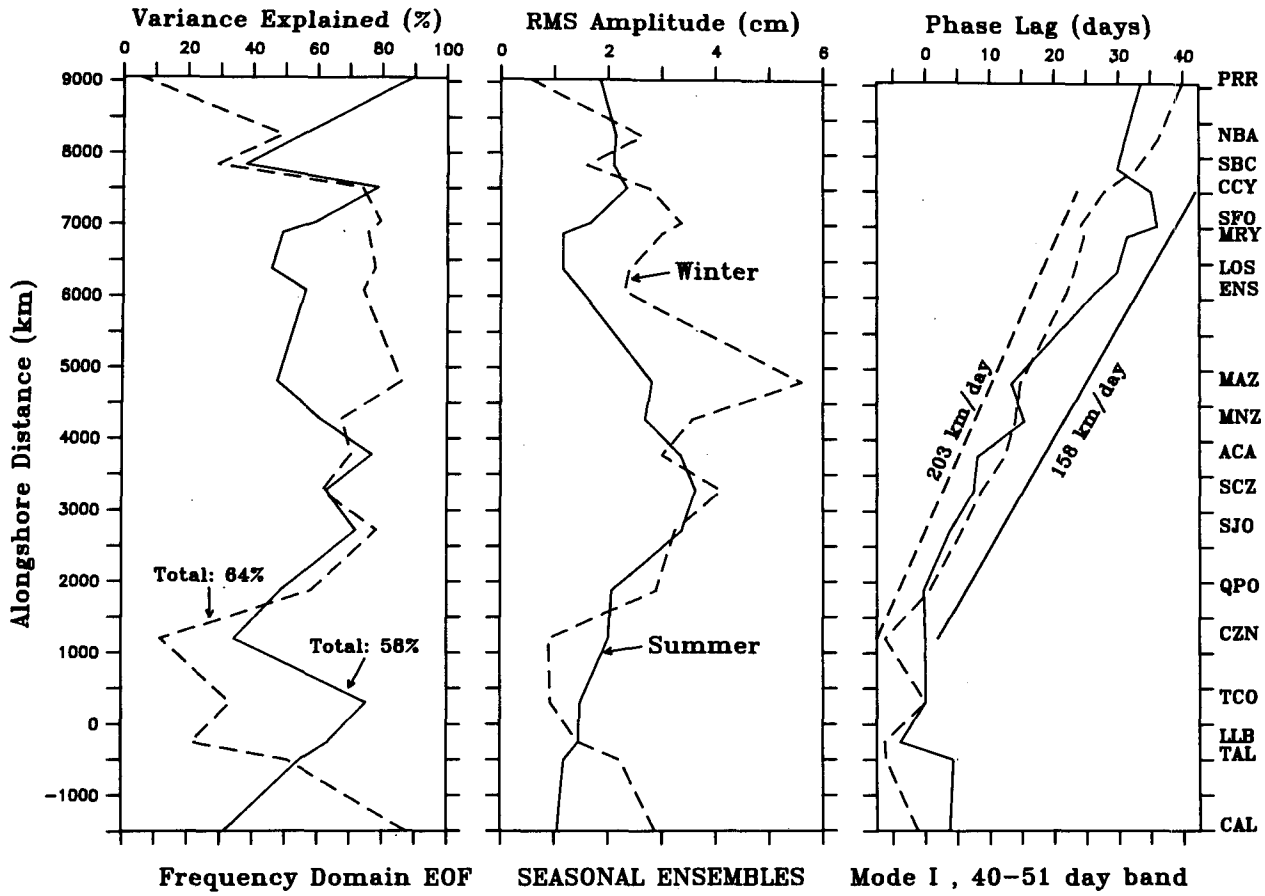

FIG. 8. Seasonal frequency domain EOFs for the poleward-propagating mode of sea level. Summer (solid curves) is defined as mid-April to mid-October and winter (dashed curves) the remainder of the year. Four realizations of each season from the 1971–75 period are ensemble-averaged resulting in 8 degrees of freedom for the 40–51 day band.

zanillo and the tip of Baja is only 350 km, small compared to the several thousand kilometer alongshore scale of intraseasonal coastal-trapped waves, diffraction is a possible mechanism for northward continuation beyond the Gulf.

The persistence or stationarity of the oscillation, identified in the above analysis, may be examined by applying an inverse Fourier transformation to the frequency components of the EOF mode (Wallace and Dickinson, 1972). For this purpose a wide-band EOF from 21 frequencies spanning the period range 36–73 days is utilized. The first mode accounts for 47% of the total variance, with the remainder spread across several minor modes. The phase structure is again consistent with poleward propagation, and the phase speed of 170 km day^{-1} does not differ from the earlier estimates at the 95% confidence level. The process of inversion to the time domain is similar to bandpass filtering by truncation in the frequency domain. Tapering at the extremes of the frequency band is applied to reduce the ringing that typically results when the FFT is applied to boxcar or Heaviside functions. The extremes of the series are not reliable, due to the Gibbs phenomenon, whereby Fourier series synthesis of a finite data record is poorest at the endpoints, owing to the implicit assumption of periodic extension. The result of the EOF inversion is shown in the lower panel of Fig. 2. The visual impression from the upper panel is confirmed, in that the intraseasonal signal is enhanced somewhat during the El Niño episode (1972–73 winter) and almost absent during the following summer. The latter feature may be the more significant. While energetic intraseasonal oscillations occur elsewhere in the record, Enfield (1987) has observed a similar decrease in the level of activity at Callao, following the 1982–83 El Niño. It has been suggested (Lau, 1985; Lau and Chan, 1986) that the intraseasonal and El Niño signals may be related. From the behaviour of a mechanical analog, Lau (1985) suggests a scenario whereby a stochastic 40–50 oscillation of the tropical atmosphere in concert with the seasonal cycle may trigger the El Niño onset.

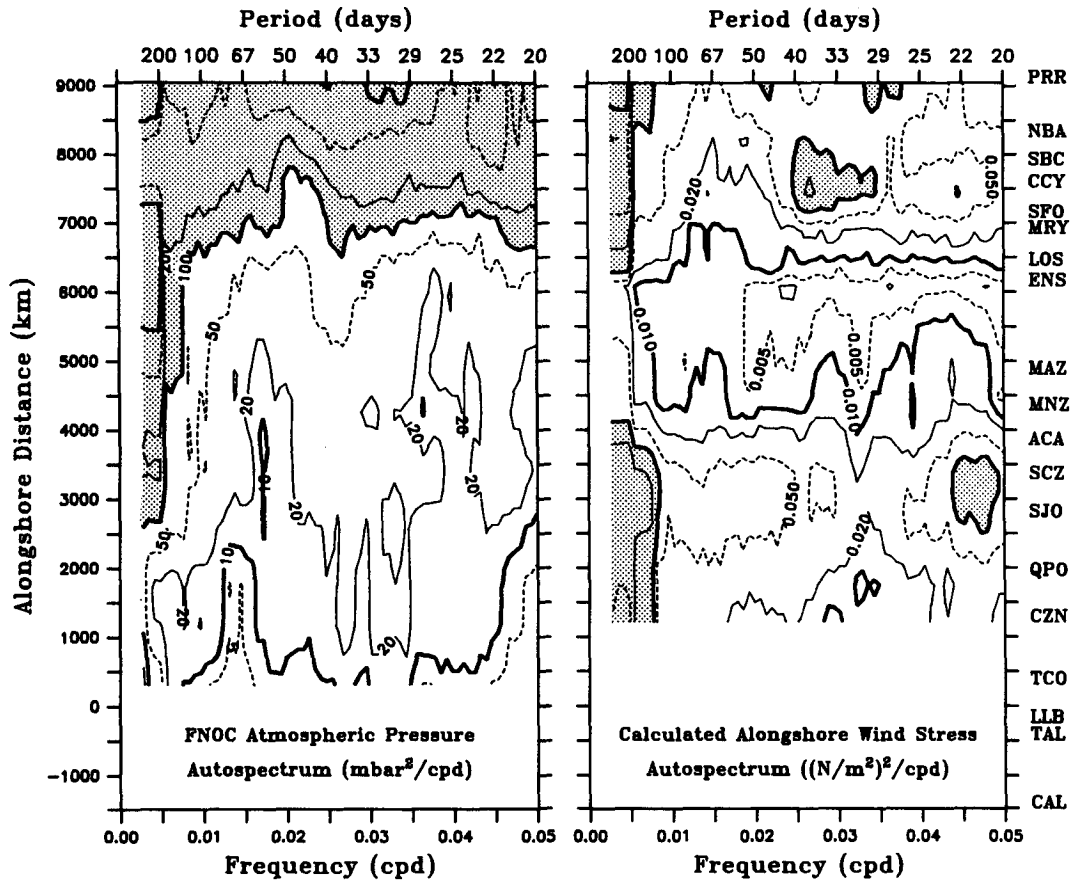

FIG. 9. Spatial structure of autospectral density for FNOC atmospheric pressure and calculated alongshore wind stress for the period 1971–75. Contour levels, in approximately logarithmic steps (1, 2, 5, 10), are expressed in units of $mb^2\ cpd^{-1}$ for pressure and $(N\ m^{-2})^2\ cpd^{-1}$ for wind stress, with values above 100 and 0.1, respectively, shaded. Estimates have 14 degrees of freedom in a moving band average. Multiplication of an autospectral estimate by 2.73 and 0.51 provide the upper and lower 95% confidence limits.

In the above analysis the spectral results were obtained by applying the FFT to the entire record of 4 years, with band-averaging applied to form estimates in each selected frequency band. To further test for seasonality in the propagating mode identified above, each year was divided into a summer section (mid-April to mid-October) and a winter portion (the remainder). Separate frequency domain EOFs are computed for each season, by ensemble-averaging the spectral estimates from each realization. The results for the 40–51 day band (8 degrees of freedom) are shown in Fig. 8. Solid and dashed lines represent the results for summer and winter, respectively. The dominant modes in both seasons, with 58% of the total variance in the band for the summer ensemble and 64% for winter, have phase distributions similar to each other and to the phase structure computed from the entire record. We conclude that the intraseasonal oscillation is an ubiquitous feature of Pacific eastern boundary sea level variability and, though its amplitude is modulated, does not appear to have any clear seasonality.

6. Meteorological influences

The spatial structures of the autospectral density for FNOC pressure and calculated alongshore wind stress are contoured in Fig. 9. South of San Francisco the pressure spectrum is red and, as noted in section 2, the overall energy decreases to the south through Mexico and Central America. North of San Francisco the pressure spectrum becomes broadband in nature. The spectrum of calculated wind stress is energetic in two regions: the region of midlatitude westerlies north of Los Angeles, and again between Manzanillo and Canal Zone, where strong northeast trades blow in winter and tropical storms occur in summer.

In the intraseasonal band, the available measures of atmospheric forcing do not reveal any organized cross-spectral structures, in the alongshore sense, comparable to those seen for sea level (Figs. 4, 5 and 6). The local coherence squared of atmospheric pressure and alongshore stress to sea level, displayed in Fig. 10, shows only scattered significant values in the intraseasonal

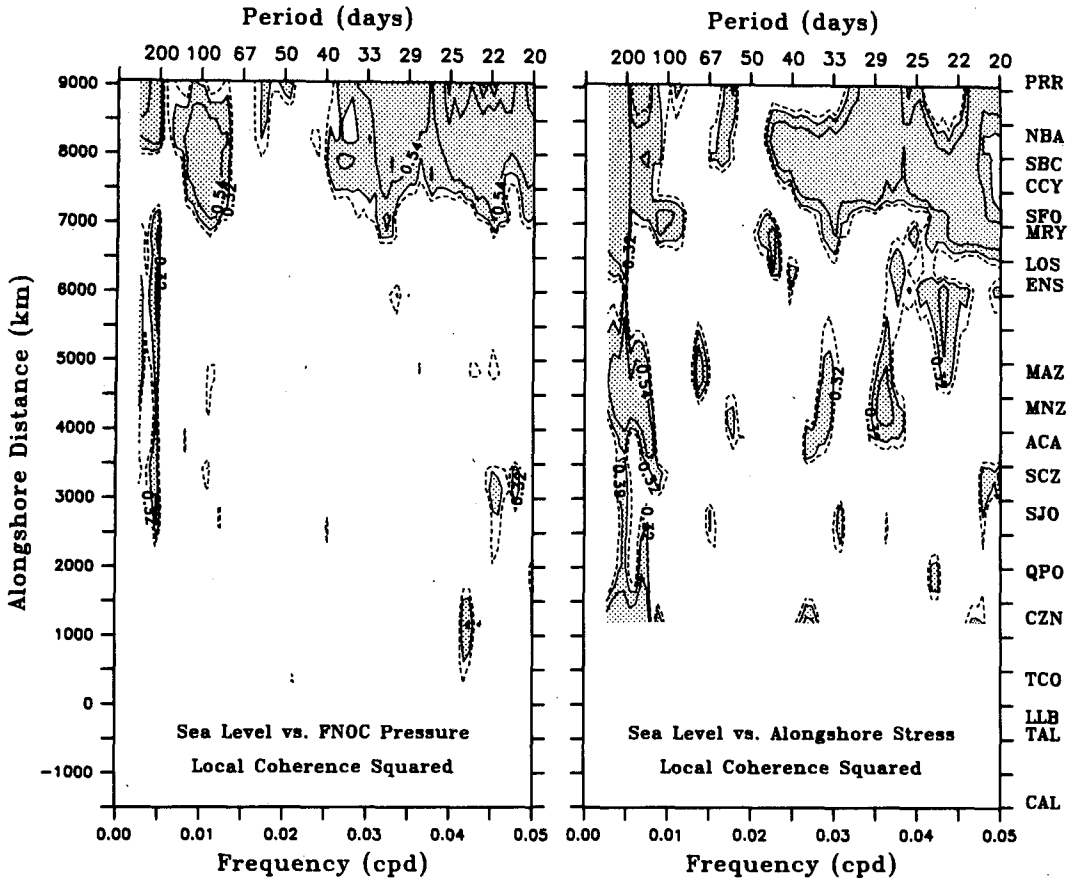

FIG. 10. Spatial structure of the local coherence squared of FNOC atmospheric pressure and calculated alongshore wind stress to sea level in the period 1971–75. Estimates have 14 degrees of freedom in a moving band average. Contours are drawn at the 90%, 95% and 99% significance levels with coherences above the 95% level shaded.

band. In particular we note the isolated high coherence between local sea level and alongshore wind stress in the region near San Francisco where the frequency domain EOF mode representing large-scale intraseasonal propagation is weakest (Fig. 7). Breaker and Lewis (1987) have observed coherence of sea surface temperature and wind stress in this region, though they report negligible coherence between daily-averaged sea level and wind stress coherence at Monterey over the period 1971–76.

The isolated high coherence values in the intraseasonal band vanish when the individual sea level station spectra are replaced by the spectral coefficients of the dominant frequency domain EOF mode for sea level in the coherence calculation. The wind stress curl, as calculated from the gridded FNOC data, was tested as another possible source of atmospheric forcing near the continental margin, with similar negative results. We conclude that there is no evidence that the poleward propagating intraseasonal oscillation, as seen in the coastal sea level record, is forced by atmospheric fluctuations in the coastal zone poleward of 9°N.

7. Conclusions

Spectral analysis techniques, applied to four years of tide gauge data, have revealed strong evidence of an intraseasonal (36–73 day periods) oscillation of sea level along the west coast of the Americas, detectable to mid-California in the Northern Hemisphere and at all available Southern Hemisphere stations. Several features of the signal suggest that it propagates poleward as a coastal wave, unforced by local meteorological influences. These features are 1) the amplitude structure near the equator, growing with latitude as the coastal deformation radius constricts; 2) the region of near-constant phase close to the equator, since coastal-trapping for 50-day waves with speeds of 150 km day^{-1} should occur only poleward of about 5°; 3) the phase speed of 150–200 km day^{-1}, consistent with predictions of linear theory (Enfield and Allen, 1983) and 4) the lack of coherence of the signal (as represented by its frequency-domain EOF) with available measures of meteorological forcing.

The energy source for this intraseasonal variability of coastal sea level is not identifiable in data available

for the 1971–75 period. However, as detailed in the Introduction, a considerable body of observations of intraseasonal variability in the tropical atmosphere exists, and several studies have reported an equatorial ocean response. Since the equatorial oceanic waveguide provides an effective conduit connecting the central Pacific with the eastern boundary, we suggest that the coastal-trapped waves revealed in this study may be yet another manifestation of the intraseasonal oscillation in the atmosphere. This hypothesis is being further investigated by Enfield (1987) using data from the 1980s, where more extensive atmospheric measurements are available.

Acknowledgments. This research was supported by the Oceanography Section of the National Science Foundation under Grant OCE-8317390. We thank G. R. Halliwell for providing the atmospheric data in a convenient format, and P. M. Newberger and H. L. Pittock for editing the sea level data. We also express our gratitude to the organizations that have provided the sea level data used in this study (Table 1).

REFERENCES

Allen, J. S., 1984: A simple model for stratified shelf flow fields with bottom friction. *J. Phys. Oceanogr.*, **14,** 1200–1214.

——, and R. D. Romea, 1980: On coastal trapped waves at low latitudes in a stratified ocean. *J. Fluid Mech.*, **98,** 555–585.

Andersen, N., 1974: On the calculation of filter coefficients for maximum entropy spectral analysis. *Geophysics,* **39,** 69–72.

Bakun, A., 1973: Coastal upwelling indices, west coast of North America, 1946–71. Tech. Rep. NMFS SSRF-671, NOAA, Seattle, 103 pp.

Beardsley, R. C., R. Limeburner and L. K. Rosenfeld, 1985: Introduction to CODE-2: Moored array and large-scale data report. R. Limeburner, Ed., WHOI Tech. Rep. 85–35, CODE Tech. Rep. 38.

Box, G. E., and G. H. Jenkins, 1970: *Time Series Analysis: Forcing and Control.* Holden-Day, 553 pp.

Breaker, L. C., and P. A. W. Lewis, 1987: A 40 to 50 day oscillation in sea surface temperature along the central California coast. Submitted to *Estuarine Coastal Shelf Sci.*

Brink, K. H., 1982: A comparison of long coastal-trapped wave theory with observations off Peru. *J. Phys. Oceanogr.*, **12,** 897–913.

Buchwald, V. T., and J. W. Miles, 1974: Kelvin-wave diffraction by a gap. *J. Aust. Math. Soc.*, **17,** 29–34.

Cane, M. A., and E. S. Sarachik, 1977: Forced baroclinic ocean motions. II: The linear equatorial bounded case. *J. Mar. Res.*, **35,** 395–432.

Chelton, D. B., P. A. Bernal and J. A. McGowan, 1982: Large-scale interannual physical and biological interaction in the California Current. *J. Mar. Res.*, **40,** 1095–1125.

——, and R. E. Davis, 1982: Monthly mean sea level variability along the west coast of North America. *J. Phys. Oceanogr.*, **12,** 757–784.

Christensen, N., Jr., R. de la Paz and G. Gutierrez, 1983: A study of sub-inertial waves off the west coast of Mexico. *Deep-Sea Res.*, **30,** 835–850.

Davis, R. E., 1976: Predictability of sea surface temperature and sea level pressure anomalies over the North Pacific. *J. Phys. Oceanogr.*, **6,** 249–266.

Enfield, D. B., 1987: The intraseasonal oscillation in Eastern Pacific sea levels: How is it forced? *J. Phys. Oceanogr.*, **17,** In press.

——, and J. S. Allen, 1980: On the structure and dynamics of monthly mean sea level anomalies along the Pacific coast of North and South America. *J. Phys. Oceanogr.*, **10,** 557–578.

——, and ——, 1983: The generation and propagation of sea level variability along the Pacific coast of Mexico. *J. Phys. Oceanogr.*, **13,** 1012–1033.

Gill, A. E., 1982: *Atmosphere-Ocean Dynamics.* Academic Press, 662 pp.

Halliwell, G. R., and J. S. Allen, 1984: Large-scale sea level response to atmospheric forcing along the west coast of North America, summer 1973. *J. Phys. Oceanogr.*, **14,** 864–886.

Krishnamurti, T. N., and D. Subrahmanyam, 1982: The 30–50 day mode at 850 mb during MONEX. *J. Atmos. Sci.*, **39,** 2088–2095.

Large, W. G., and S. Pond, 1981: Open ocean flux measurements in moderate to strong winds. *J. Phys. Oceanogr.*, **11,** 324–336.

Lau, K. M., 1985: Sub-seasonal scale oscillation, bimodal climatic state and the El Niño/Southern Oscillation. *Coupled Ocean-Atmosphere Models,* J. Nihoul, Ed., *Elsevier Oceanogr. Ser.*, **40,** 29–40.

——, and P. H. Chan, 1986: The 40–50 day oscillation and the El Niño/Southern Oscillation: A new perspective. *Bull. Amer. Meteor. Soc.*, **67,** 533–534.

Luther, D. S., 1980: Observations of long period waves in the tropical oceans and atmosphere. Ph.D. dissertation, Joint Program in Oceanography, Massachusetts Institute of Technology and the Woods Hole Oceanographic Institution, 210 pp.

McCreary, J., 1976: Eastern tropical ocean response to changing wind systems with application to El Niño. *J. Phys. Oceanogr.*, **6,** 632–645.

Madden, R. A., and P. R. Julian, 1971: Detection of a 40–50 day oscillation in the zonal wind field in the tropical Pacific. *J. Atmos. Sci.*, **28,** 702–708.

——, and ——, 1972: Description of global-scale circulation cells in the tropics with a 40–50 day period. *J. Atmos. Sci.*, **29,** 1109–1123.

Mertz, G. J., and L. A. Mysak, 1984: Evidence for a 40–60 day oscillation over the western Indian Ocean during 1976 and 1979. *Mon. Wea. Rev.*, **112,** 383–386.

Moore, D. W., and S. G. H. Philander, 1977: Modelling of the tropical ocean circulation. *The Sea, Vol. 6,* E. D. Goldberg and co-Editors, Wiley-Interscience.

Mysak, L. A., and G. J. Mertz, 1984: A 40- to 60-day oscillation in the source region of the Somali Current during 1976. *J. Geophys. Res.*, **89,** 711–715.

Picaut, J., and J. M. Verstraete, 1976: Mise en évidence d'une onde de 40–50 jours de période sur les côtes du Golfe de Guinée. *Cah. O.R.S.T.R.O.M., sér. Océanogr.*, **14,** No. 1, 3–14.

Quinn, W. H., 1974: Monitoring and predicting El Niño invasions. *J. Appl. Meteor.*, **13,** 825–830.

Schott, F., and W. Düing, 1976: Continental shelf waves in the Florida Straits. *J. Phys. Oceanogr.*, **6,** 451–460.

Smith, R. L., 1978: Poleward propagating perturbations in currents and sea levels along the Peru coast. *J. Geophys. Res.*, **83,** 6083–6092.

Wallace, J. M., and R. E. Dickinson, 1972: Empirical orthogonal representation of time series in the frequency domain. Part I: Theoretical considerations. *J. Appl. Meteor.*, **11,** 887–892.

Weickmann, K. M., 1983: Intraseasonal circulation and outgoing longwave radiation modes during Northern Hemisphere winter. *Mon. Wea. Rev.*, **111,** 1838–1858.

Wyrtki, K., 1975: El Niño—the dynamic response of the equatorial Pacific Ocean to atmospheric forcing. *J. Phys. Oceanogr.*, **5,** 572–584.